RSC Advances

ROYAL SOCIETY OF CHEMISTRY

PAPER

View Article Online
View Journal | View Issue

Check for updates

Cite this: *RSC Adv.*, 2021, **11**, 15231

Design of a novel poly(aryl ether nitrile)-based composite ultrafiltration membrane with improved permeability and antifouling performance using zwitterionic modified nano-silica

Qi Wang, Fengna Dai, Shangying Zhang, Mengxia Wang, Chunhai Chen and Youhai Yu *

Received 16th January 2021
Accepted 17th April 2021

DOI: 10.1039/d1ra00376c

rsc.li/rsc-advances

Zwitterionic nano-silica (SiO_2 NPs) obtained by lysine surface modification was used as a hydrophilic inorganic filler for preparing a poly(aryl ether nitrile) (PEN) nanocomposite membrane *via* an immersion precipitation phase inversion method. The effects of zwitterionic SiO_2 NPs addition on the morphology, separation and antifouling performance of the synthesized membranes were investigated. Zwitterionic surface modification effectively avoided the agglomeration of SiO_2 NPs. The PEN/zwitterionic SiO_2 NPs composite membranes exhibited improved porosity, equilibrium water content, hydrophilicity and permeability due to the introduction of hydrophilic SiO_2 NPs in the casting solution, and the optimal pure water flux was up to 507.2 L m^{-2} h^{-1}, while the BSA rejection ratio was maintained at 97.4%. A static adsorption capacity of 72.9 μg cm^{-2} and the FRR up to 85.3% in the dynamic antifouling experiment proved that the introduction of zwitterionic SiO_2 NPs inhibited irreversible fouling and enhanced the antifouling ability of the PEN membrane.

1. Introduction

Membrane separation technology has extensive applications in various fields such as pharmaceuticals,[1] biotechnology,[2] food,[3] fuel cells,[4] and especially water treatment,[5,6] owing to its advantages of being effective, low energy consumption, easy operation, no pollution, *etc*[7]. The filtration accuracy of ultrafiltration is between microfiltration and nanofiltration. It is usually defined as a membrane with an average pore diameter in the range from 10 A to 1000 A for effective filtration of organic substances, such as proteins, viruses, *etc*[8–10]. Generally, according to the composition of the membrane material, UF membranes can be divided into ceramic membranes and polymeric membranes. Polymeric membrane has become preferred choice for preparing applied UF membrane due to its controllable structure and simple preparation process. Typical polymeric membrane materials include polysulfone (PSf),[11,12] poly(ether sulfone) (PES),[13] poly(vinylidene fluoride) (PVDF),[14–16] polyimides (PI),[17] cellulose acetate (CA)[18] and polyacrylonitrile (PAN),[19] all of which have good mechanical properties, physicochemical resistance and thermal stability. As a semi-crystalline special engineering plastic, PEN is widely used in automotive, electronics, military, and aerospace fields due to its excellent mechanical properties, good thermal stability, excellent radiation resistance, physical and chemical resistance.[20–22] In recent years, it has also been used to in water treatment.[23,24] However, due to their inherent hydrophobicity, both PEN and traditional polymeric membrane materials suffer from the problem of membrane fouling.[25] Thus, the preparation of polymeric membrane with excellent antifouling properties has been a hot topic.

Research shows that during the filtration process, the hydrophilic polymeric membrane is more likely to form hydration layer on the surface, which effectively weakens the interaction between hydrophobic contaminants and membrane surface. Simultaneously, due to the barrier of hydrated layer, the pollutants deposited on the membrane surface is easier to wash off, thereby greatly improving the antifouling performance of the membranes.[26–28] Several modification methods include blending,[29–31] coating,[32] surface grafting[33,34] and bulk modification,[35] have been developed to improve the hydrophilicity of the polymeric membranes. Among them, blending, especially the physical blending with hydrophilic nanoparticle materials to prepare mixed matrix membranes (MMMs) with improved hydrophilicity has been wildly adopted due to the advantage of easy operation.

SiO_2 NPs, a common inorganic filler with the benefits of non-toxic, long-term stability, high specific surface area and hydrophilicity, has been widely used to adjust the permeability and

---

Center for Advanced Low-Dimension Materials, State Key Laboratory for Modification of Chemical Fibers and Polymer Materials, College of Material Science and Engineering, Donghua University, Shanghai 201620, P. R. China. E-mail: yuyouhai@dhu.edu.cn

antifouling properties of polymeric membranes.[36–38] SiO_2 NPs with high specific surface area usually causes particle agglomeration due to their high surface energy, and thus exhibit a poor dispersion stability, which greatly hinders the appearance of their nano-scale material characteristics.[39] Zwitterionic material refers to an amphoteric polymer with positive and negative charge groups on the same monomer.[40] Lysine is a cheap, non-toxic, and environmentally friendly zwitterionic amino acid which has excellent hydrophilicity.[41] For lysine in the zwitterionic state, H protons in the –COOH in the non-ionized state are transferred to the $-NH_2$ terminal to form amphoteric ions with both $-NH^{3+}$ and $-COO^-$. The silane coupling agent KH560, containing oleophilic epoxy terminal and inorganic silane terminal, is commonly used for SiO_2 surface modification.[42,43] The inorganic silane terminal can tightly link with SiO_2 through dehydration and condensation, while the oleophilic epoxy terminal can bound with specific organics through the ring-opening reaction.[44,45] Using KH560 as a connecting medium, lysine can be grafted onto the SiO_2 NPs surface to realize the zwitterionization of nanoparticles. On one hand, since SiO_2 surface was coated with zwitterionic long chain, it effectively weakened the hydrogen bonding between the adjacent –OH on the nanoparticles surface, and also generated steric hindrance, which ultimately reduced the agglomeration between nanoparticles.[46] On the other hand, due to the strong solvation and hydrogen bonding characteristics of the zwitterionic chain end groups, it is more conducive to the formation of a dense hydration layer on the surface, thus reducing the non-specific adsorption with proteins.[47,48]

In this work, lysine was used as a surface modifier for the preparation of zwitterionic SiO_2 NPs to promote the dispersion stability and hydrophilicity of nanoparticles in the casting solution system.[49] PEN flat sheet composite membranes with different concentration of zwitterionic SiO_2 NPs were prepared by immersion precipitation phase inversion method with PVP-k30 as pore-forming agent and a mixture of DMAc and NMP as solvent. The effects of zwitterionic SiO_2 NPs addition on the morphology, separation and antifouling performance of the synthesized membranes were investigated in detail.

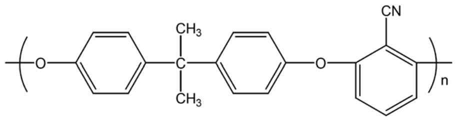

Poly (aryl ether nitrile)

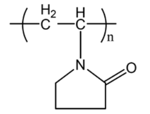

Polyvinylpyrrolidone

Fig. 1 Molecular structure of poly(aryl ether nitrile) and polyvinylpyrrolidone.

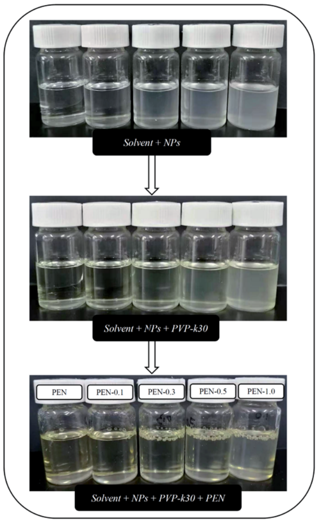

Fig. 2 The real situation of the casting solution in different states.

2. Experimental

2.1. Materials

PEN ($[\eta]$ = 1.15 dL g^{-1}) synthesized in the laboratory as described in previous literature[50] was used as the base polymer in the casting solution. Reagent grade PVP-k30 supplied by Macklin Biochemical Technology Co. Ltd. was used as pore-forming agent. The chemical structure of PEN and PVP were shown in Fig. 1. Reagent grade DMAc (≥99.8% purity) and NMP (≥99.5% purity) supplied by Macklin, were used as mixed solvent without further purification. SiO_2 NPs (7–40 nm, hydrophilic-380 type) and 3-glycidyloxypropyl (dimethoxy) methylsilane (GPMS, KH560) were obtained from Aladdin Biochemical Technology Co. Ltd. Lysine, Hydrochloric acid, Ethanol were purchased from Sinopharm Group Chemical Reagent Co. Ltd. Bovine serum albumin (BSA) with molecular weight of 68 000 Da was obtained from Energy Chemical Co. Ltd. Deionized water purified with Millipore system (Millipore, France) was used as the coagulation bath.

2.2. Surface modification of nano-silica

Surface modification of SiO_2 NPs was performed to overcome agglomeration and improved its dispersion. Firstly, 1.0 g SiO_2 NPs were dispersed into a 50 mL (20%, v/v) ethanol aqueous solution by ultrasound for 0.5 h. Then, 0.3 g GPMS and several drops of hydrochloric acid were added into the solution to react with a magnetic stirring at 60 °C for 6 h. Subsequently, 5 mL (10%, g g^{-1}) lysine aqueous solution was added into the above solution to keep reaction for another 3 h. Finally, the modified nano-SiO_2 was washed several times to neutrality by centrifugation with ethanol, and then thoroughly dried in a vacuum oven at 80 °C for use.

2.3. Preparation of PEN nanocomposite membranes

PEN nanocomposite membranes were prepared by immersion precipitation phase inversion method. Firstly, a certain amount of zwitterionic SiO_2 NPs was dispersed in a mixed solvent of

Table 1 Composition of the casting solution and their viscosities

Membranes	Polymer (wt%) PEN	Pore-forming agent (wt%) PVP-k30	Nanoparticles (wt%) zwitterionic SiO_2	Solvent (wt%) DMAc : NMP = 4 : 1	Suspension viscosity, (cP)
Pristine PEN	16	8	0.0	76.0	18 479
PEN-0.1	16	8	0.1	75.9	18 823
PEN-0.3	16	8	0.3	75.7	19 576
PEN-0.5	16	8	0.5	75.5	20 382
PEN-1.0	16	8	1.0	75.0	21 268

DMAc and NMP through ultrasonication for 3 h to obtain a stable dispersion while more than 1 wt% of SiO_2 NPs would lead to a poor dispersion stability in the solvent. Then, 8 wt% of PVP-k30 was dissolved by stirring. Subsequently, 16 wt% of PEN was added and completely dissolved to form a uniform solution by continuous stirring at 60 °C. The real situation of each casting solution in different states were shown in Fig. 2. Furthermore, defoaming was performed for 0.5 h to remove air bubbles. Finally, the casting solution was spread uniformly on a clean glass plate with the help of a casting knife maintaining a clearance of approximately 100 μm between the knife and glass plate at room temperature and relative humidity $\leq$50%. The prepared membrane was then exposed for about 25 s in ambient before immersion into the coagulation bath of deionized water (DI water). The casted films changed color from transparent to white immediately and separated out of the glass after a while. Then, the prepared membrane was kept and saved in DI water for a complete liquid–liquid separation. Finally, the flat sheet membranes were cut into a rectangle (8.50 cm × 3.50 cm) to place inside the membrane cell. All samples were visually inspected for defects and used for membrane evaluation.

Membranes with different concentration of zwitterionic nano-SiO_2 were designated as Pristine PEN, PEN-0.1, PEN-0.3, PEN-0.5 and PEN-1.0. Table 1 represented the composition and viscosities of each casting solution. The concentration of PEN kept constant at 16 wt%, while PVP-k30 kept at 8 wt%, DMAc : NMP = 4 : 1 as a mixed solvent.

2.4. Characterization of zwitterionic nano-silica

The particle size distribution and zeta potential before and after the modification of nano-SiO_2 was tested by the zeta-potential analysis and particle size analyzer (Nano ZS, Malvern). The chemical compositions of nanoparticles were characterized by Fourier transform infrared spectroscopy (FTIR, VERTEX70) at a scanning range of 400–4000 cm^{-1}, and X-ray photoelectron spectroscopy (XPS, Escalab 250Xi). The dispersion stability of nano-SiO_2 before and after modification in water was assessed by natural gravimetric sedimentation over a period of time in static mode.

2.5. Characterization of membrane

The surface and cross-section morphology of resulting membranes were observed by a field emission scanning electron microscope (SEM, *Regulus8230) with energy dispersive X-ray spectroscopy (EDX). All specimens were freeze-dried and coated with a thin layer of gold before observation. Cross-section was prepared by fracturing membrane in liquid nitrogen.

The surface morphology (2D and 3D topographic images) and roughness analysis of mean roughness (R_a) and the root mean square of data (R_q) for each nanocomposite membrane in a scan area of 5 μm × 5 μm were characterized using an atomic force microscope (AFM, *MFP-3D Bio) at the acoustic AC tapping mode.

Equilibrium water content (EWC) and porosity (ε) were calculated by the gravimetric method as follows:

$$\text{EWC}\,(\%) = (W_w - W_d)/W_w \times 100\% \tag{1}$$

$$\varepsilon\,(\%) = (W_w - W_d)/\rho_w A l \times 100\% \tag{2}$$

where, W_w and W_d is weight of membranes in a wet and dry state (g). ρ_w, A, and l are the density of pure water (0.998 g cm^{-3}), effective membrane surface area (cm^2), and membrane thickness (cm), respectively.

The mean pore radius (r_m) for blended membranes were calculated using the Guerout–Elford–Ferry equation:

$$r_m = \sqrt{[(2.9 - 1.75\varepsilon) \times 8\eta l J_w]/(\varepsilon \Delta P)} \tag{3}$$

where, ε is porosity of the membrane, η is the viscosity of water (8.9×10^{-4} Pa s), l is the mean thickness of membrane, J_w is the pure water flux, and ΔP is the operating pressure (0.1 MPa).

The water contact angle (WCA) of membranes was measured using a Drop Shape Analysis Data physics (OCA 20) at room temperature. The water droplet of 2 μL was dropped on membrane surface using motorized controlled micro-syringe. The image of water droplet on membrane surface was captured and surface water contact angle was measured by using imaging software. The contact angle was measured at lots of random points on membrane surface and reported value was the average of these measurements.

The surface energy parameters (γ_s) of the membrane were determined by the Lifshitz–van der Waals (γ_s^{LW}) and Lewis acid–base (γ_s^{AB}) (comprising electron-donor γ_s^- and electron-acceptor γ_s^+) was determined with eqn (4).

$$\gamma_s = \gamma_s^{LW} + \gamma_s^{AB} = \gamma_s^{LW} + 2\sqrt{\gamma_s^- \times \gamma_s^+} \tag{4}$$

Contact angle measurements were performed using three different types of probe liquids with known surface energy, in which the water and formamide represent polar liquids, the diiodomethane is a nonpolar liquid. And then, γ_s was calculated by solving a set of extended Young–Dupré eqn (5).

$$(1+\cos\theta)\gamma_{\mathrm{L}} = 2\left(\sqrt{\gamma_{\mathrm{s}}^{\mathrm{LW}}\times\gamma_{\mathrm{L}}^{\mathrm{LW}}}+\sqrt{\gamma_{\mathrm{s}}^{+}\times\gamma_{\mathrm{L}}^{-}}+\sqrt{\gamma_{\mathrm{s}}^{-}\times\gamma_{\mathrm{L}}^{+}}\right) \quad (5)$$

where, θ represents the contact angle of the liquid on a solid surface, and subscripts S and L represent the solid surface and the liquid surface, respectively.

2.6. Ultrafiltration experiments

The batch experiments were conducted in a crossflow filter (FMT FlowMem-0002). Inside the cell, a rectangular membrane was placed over a base support, the effective filtration area of the membrane was 20 cm^2. Under the pressure of the diaphragm pump, the permeate was collected from the bottom of the cell. The schematic of batch experimental was presented in Fig. 3.

Fresh membranes need to be compacted with pure water for 0.5 h at a transmembrane pressure of 0.2 MPa. This pressure is twice than normal operating pressure, which helps to improve the mechanical strength of the membrane and obtain stable water flux. Under the pressure of 0.1 MPa, the pure water flux (PWF) and hydraulic permeability (P_{m}) were calculated, using the following equations:

$$J_{\mathrm{w}} = Q/(A\times\Delta T) \quad (6)$$

$$P_{\mathrm{m}} = J_{\mathrm{w}}/\Delta p \quad (7)$$

where, J_{w} is pure water flux (L m^{-2} h^{-1}), Q is volume of water permeated (L), A is effective membrane area (m^2) and ΔT is sampling time (h). P_{m} is hydraulic permeability (L m^{-2} h^{-1} kPa^{-1}); ΔP is transmembrane pressure(kPa).

Followed by pure water flux measurement, the DI water was replaced with model protein solution (1000 mg L^{-1} of BSA in phosphate buffer solution, pH = 7.4) to evaluate the rejection ratios of membranes. Percentage rejection of BSA was calculated using the following equation:

$$R\,(\%) = (1 - C_{\mathrm{p}}/C_{\mathrm{f}})\times 100\% \quad (8)$$

where, C_{p} and C_{f} are the concentrations in the permeate and feed (mg L^{-1}), respectively. The BSA concentration in the permeate was determined using a UV-vis spectrophotometer (PerkinElmer Precisely, Lambda950) at a wave length of 278.5 nm.

2.7. Antifouling test

The antifouling ability of separation membrane was usually evaluated by static adsorption and dynamic antifouling experiment of common pollutants. The static adsorption test was carried out by immersing membrane (2 × 2 cm^2) in a BSA solution (1000 mg L^{-1}, pH = 7.4) without additional pressure assisted pollutant into the membrane pore. After adsorption–desorption equilibrium for 24 h at room temperature, the concentrations of BSA solution before and after adsorption were measured with a UV-vis spectrophotometer (PerkinElmer Precisely, Lambda 950), and the adsorption mass Q (μg cm^{-2}) of BSA on membrane surface was calculated using the following equation:

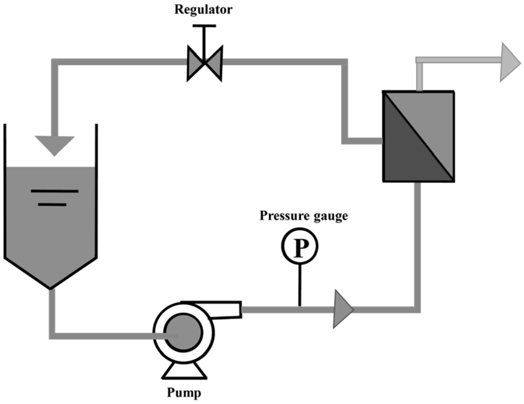

Fig. 3 Schematic of the experimental set-up.

$$Q = (C_0 - C)V/S\times 100\% \quad (9)$$

where, C_0 and C are the concentration of BSA solution before and after adsorption (mg L^{-1}), respectively, V is the volume of BSA solution (L), S is the adsorption membrane area (cm^2).

The dynamic fouling experiment was conducted using three cycles of alternating feeding of pure water and pollutants solution. The specific operations of three processes in a cycle are as follows: firstly, under the driving pressure of 0.1 MPa, the pure water flux (F_{w1}) of compacted membrane was measured for 45 min. Then followed by 1 mg mL^{-1} BSA solution as feed for another 45 min, the stable permeation flux was recorded as F_{p}. After that, the membrane was washed and backwashed with pure water for 20 min to completely remove the effects of reversible fouling. Finally, measure the pure water flux (F_{w2}) again within 45 min. Three cycles of antifouling test for each membrane were conducted. The total fouling ratio (R_{t}), reversible fouling (R_{r}), irreversible fouling (R_{ir}) and flux recovery ratio (FRR) were calculated using eqn (10)–(13), respectively:

$$R_{\mathrm{t}}\,(\%) = (1 - F_{\mathrm{p}}/F_{\mathrm{w1}})\times 100\% \quad (10)$$

$$R_{\mathrm{r}}\,(\%) = [(F_{\mathrm{w2}} - F_{\mathrm{p}})/F_{\mathrm{w1}}]\times 100\% \quad (11)$$

$$R_{\mathrm{ir}}\,(\%) = [(F_{\mathrm{w1}} - F_{\mathrm{w2}})/F_{\mathrm{w1}}]\times 100\% \quad (12)$$

$$\mathrm{FRR}\,(\%) = F_{\mathrm{w2}}/F_{\mathrm{w1}}\times 100\% \quad (13)$$

where, F_{w1} is the pure water flux, F_{p} is the permeation flux of BSA solution, and F_{w2} is pure water flux of cleaned membrane (L m^{-2} h^{-1}).

2.8. Mechanical performance test

Ultrafiltration is a pressure-driven process, the mechanical strength of nanocomposite membrane was measured including breaking strength and elongation at break, using Universal testing machine (Instron USA, capacity: 10 kN). For each measurement, the sample of 30 mm length and 5 mm width was used. All the tensile tests were carried out on dry membranes with stretching rate of 1 mm min^{-1} at room temperature.

3. Results and discussion

3.1. Preparation and characterization of zwitterionic nano-silica

The schematic diagram of the reaction principle of modified nano-SiO_2 by lysine zwitterionic material was shown in Fig. 4. Firstly, the KH560 hydrolyzed under acidic conditions rapidly dehydrated and condensed with hydroxyl groups on the surface of SiO_2 to form an intermediate product with active epoxy groups. Subsequently, the ring-opening polymerization between the active amino group on the lysine molecular chain and the epoxy group on the surface of SiO_2 was used to graft lysine with a pair of amino and carboxyl functional groups to the surface of the silica nanoparticles.[51]

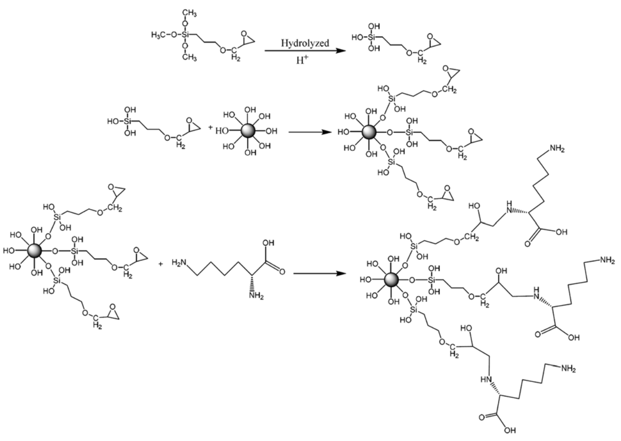

Fig. 4 Schematic diagram of nano-SiO_2 zwitterionic modification.

FTIR spectra of nano-SiO_2 before and after lysine modification were shown in Fig. 5a. The typical absorption peaks for SiO_2 at 1106 cm^{-1}, 970 cm^{-1} and 806 cm^{-1} could be seen in both spectra, which were attributed to the asymmetric and symmetric stretching vibration of Si–O–Si and the Si–OH bending vibration, respectively. Three new peaks at 2940 cm^{-1}, 1508 cm^{-1}, 1409 cm^{-1} appeared on the modified nano-SiO_2 spectrum were belong to the methylene stretching vibration peak, amino shear vibration peak, and carboxyl OH bond plane bending vibration peak. The characteristic element N of lysine could be detected in the XPS spectrum of modified SiO_2 nanoparticles as shown in Fig. 5b. All these results proved the successful preparation of zwitterionic nano-SiO_2.

In order to study the effect of zwitterionic modification on the agglomeration of nano-SiO_2 particles, the dispersion stability of the 1 mg mL^{-1} nano-SiO_2 aqueous suspension before and after modification in static mode was evaluated by natural gravimetric

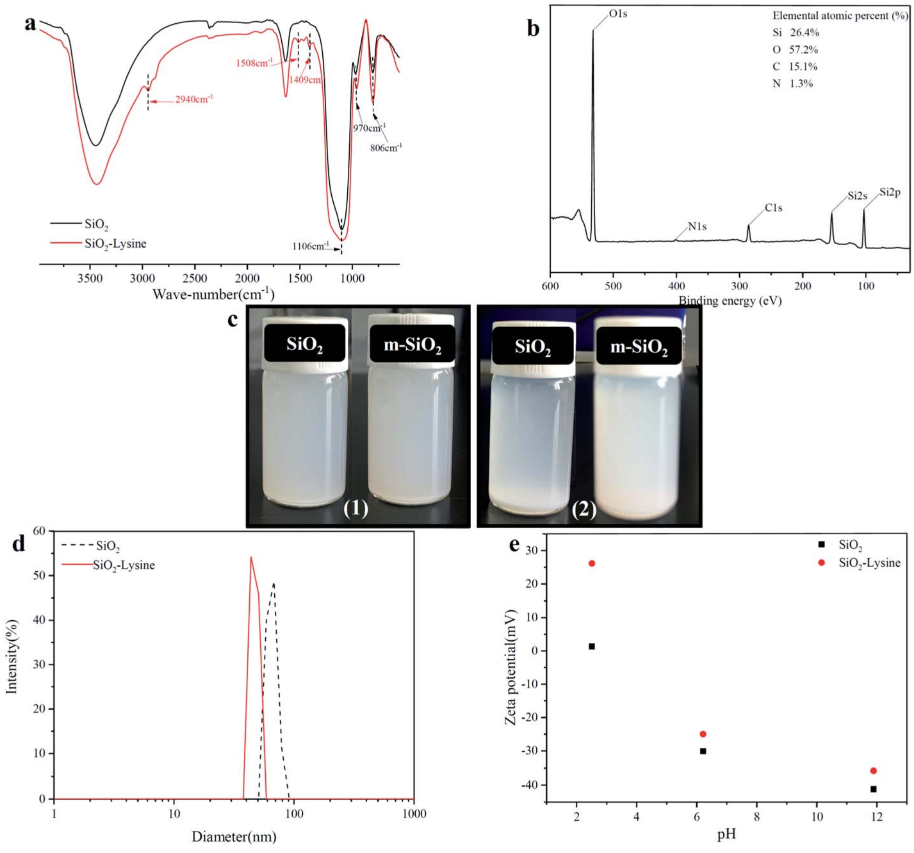

Fig. 5 Characterization of pristine and lysine modified nano-SiO_2 [(a) FTIR, (b) XPS of zwitterionic nano-SiO_2, (c) dispersion stability in water (1) just after 30 min sonication; (2) after 8 h, (d) particle size, (e) zeta potential].

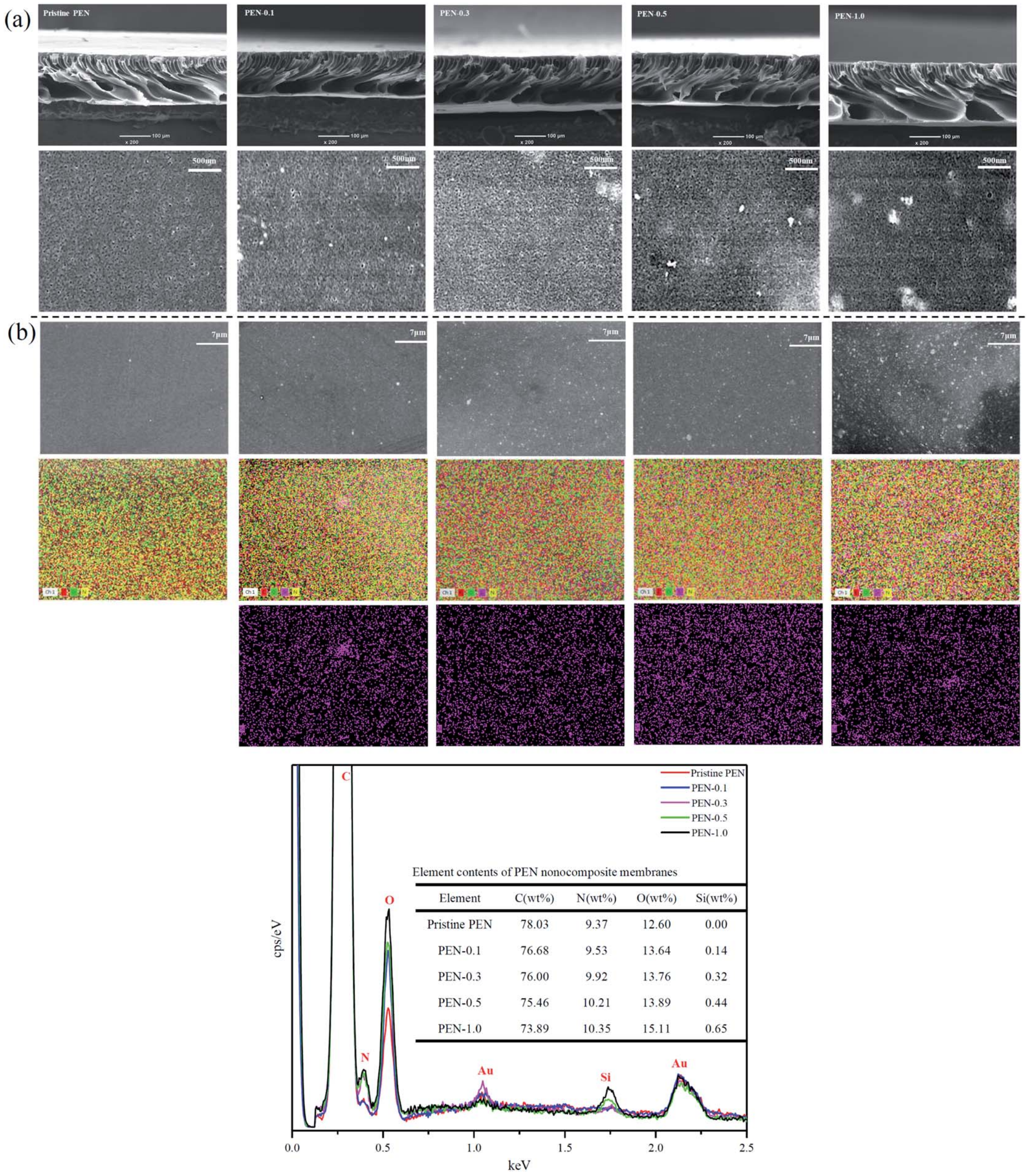

Element contents of PEN nonocomposite membranes

Element	C(wt%)	N(wt%)	O(wt%)	Si(wt%)
Pristine PEN	78.03	9.37	12.60	0.00
PEN-0.1	76.68	9.53	13.64	0.14
PEN-0.3	76.00	9.92	13.76	0.32
PEN-0.5	75.46	10.21	13.89	0.44
PEN-1.0	73.89	10.35	15.11	0.65

Fig. 6 (a) SEM images of cross-section and top surface (air-side) morphology; (b) EDX of the nanocomposite membranes.

sedimentation and the particle size distribution change of nano-SiO_2 was measured and the results are shown in Fig. 5c and d. The nano-SiO_2 before and after zwitterionic modification can obtain a uniformly dispersed suspension after 30 minutes of ultrasound. After 8 h, the pristine nano-SiO_2 particle agglomerated and precipitated, while zwitterionic nano-SiO_2 still maintained good dispersion stability. Also, the average size of SiO_2 nanoparticles is reduced from the original 66 to 47 nm after modification. This can be explained that ionogenic pair of amino and carboxyl groups introduced by the zwitterionization of SiO_2 NPs reduced the absolute value of nanoparticles surface charge, leading to a better dispersion effect.[49] Therefore, zwitterionic modification of SiO_2 can improve its dispersibility in solution. The change of zeta potential before and after modification of SiO_2 nanoparticles at different pH was shown in Fig. 5e. Compared with the pristine nano-SiO_2, lysine modified nano-SiO_2 was positively charged but showed a negative charge in a high pH environment, which is the salient feature of zwitterionic materials.

3.2. Viscosity of the casting solution

The relationship between the suspension viscosity and zwitterionic nano-SiO_2 concentration has been listed in Table 1, the apparent viscosity of the casting solution gradually increased with increasing zwitterionic nano-SiO_2 content. The increasing viscosity of the casting solution can be mainly attributed to the interaction between the polymer molecular chains and the hydroxyl groups enriched on surface of the modified silica nanoparticles with high specific surface area and surface energy.[52,53]

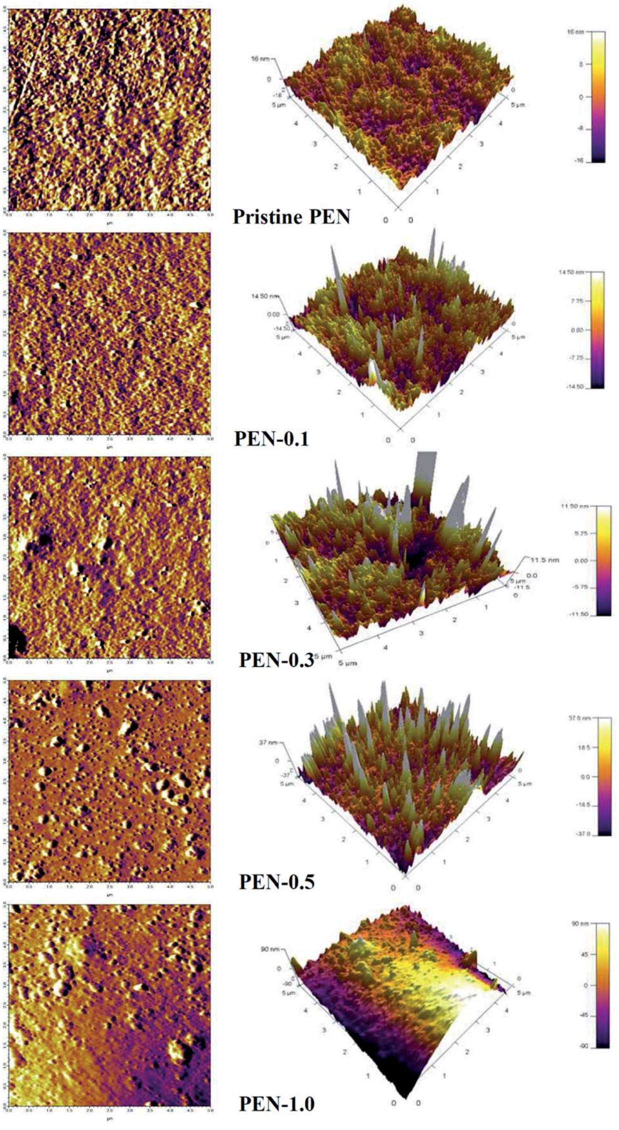

Fig. 7 AFM 2D and 3D images of PEN and zwitterionic nano-SiO_2/PEN nanocomposite membranes.

Table 2 Structural parameters of pristine PEN and nanocomposite membranes

	Structure parameters				
Membranes	R_q (nm)	R_a (nm)	EWC (%)	ε (%)	r_m (nm)
Pristine PEN	3.6	2.9	73.7	66.5	42.7
PEN-0.1	5.0	3.9	75.2	68.5	45.6
PEN-0.3	9.7	5.1	79.6	72.8	47.6
PEN-0.5	14.1	9.9	83.0	76.1	52.1
PEN-1.0	45.0	35.3	81.8	69.1	45.5

3.3. Membrane morphology and structure characterization

The cross-sectional and top surface morphologies of the pristine PEN and PEN-SiO_2 nanocomposite membranes were observed by Fig. 6a. A typical asymmetric structure with a dense skin and a finger-like cavity of the sublayer could be observed from the cross-section morphology in both pristine PEN membrane and silica hybrid membranes. The result showed that when the addition of SiO_2 was $\leq$1 wt%, there was no significant effect on the structure of membrane sublayer. The observed behavior was consistent with the results reported in the literature.[54,55] In a higher magnification surface electron micrograph, the micropores on the prepared nanocomposite membrane surface were clearly visible and evenly distributed, thus playing the role of sieving for permeation separation. Actually, when the addition of nanoparticles reached 1 wt%, the agglomeration of nanoparticles on the membrane surface was more obvious, and the defects were more likely to be observed at the edges of the agglomerated nanoparticles. This could be interpreted in accordance with the previous literature as the interface tension between organic phase and inorganic phase caused by the contraction of organic phase during phase separation process, could only be alleviated by the formation of the interface pores.[56] As shown in Fig. 6b, the EDX test confirmed the existence of silicon (Si) element in the PEN/SiO_2 nanocomposite membranes, and quantitatively proved that the SiO_2 NPs contents on the membrane surface increased with the increase of the initial addition of nanoparticles.

AFM analysis was carried out to further investigate the surface topology and roughness of the membranes. Generally, membranes with a rougher surface were prone to fouling more easily as their surfaces had more bulges and valleys which provided deposition sites for foulants.[57] Fig. 7 represented the surface 2D and 3D AFM images of the pristine PEN and nanocomposite membranes. High peak with brighter areas corresponded to nodule, while the pore or low valley was characterized by the dark regions. The surface roughness explained in terms of the root-mean-square roughness (R_q) and mean roughness (R_a) were listed in Table 2, The pristine PEN membrane had the smoothest surface, and the surface roughness increased with the increasing zwitterionic nano-SiO_2 present on top layer. Moreover, with the agglomeration of nanoparticles became more obvious, the roughness of the membranes surface increased.

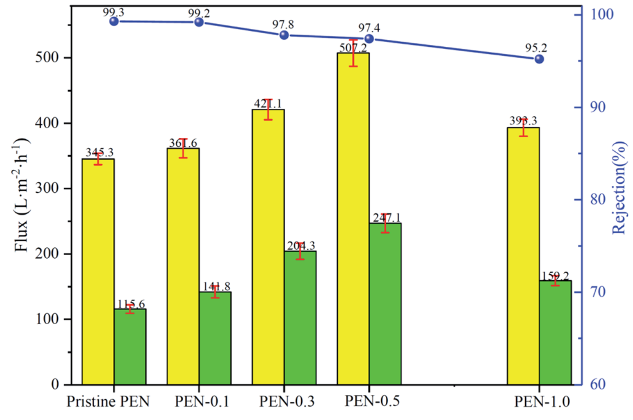

Fig. 8 Effect of zwitterionic nano-SiO_2 content on Flux and BSA rejection.

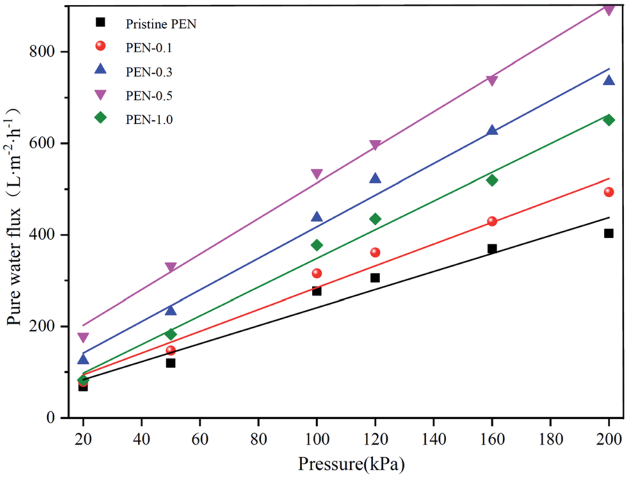

Fig. 9 Effect of zwitterionic nano-SiO_2 content on membrane P_m.

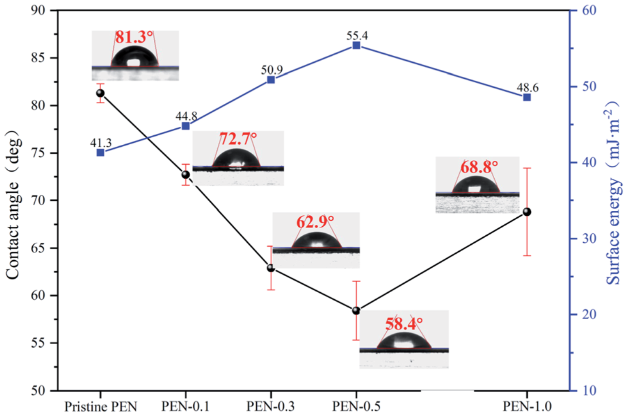

Fig. 10 Water contact angle and surface energy of pristine PEN and nanocomposite membranes.

EWC is an important parameter to reflect the ability of the membrane to hold moisture, which is related to ε and mainly determined by the macrovoids in the membrane.[58] As shown in Table 2, the incorporation of zwitterionic nano-SiO_2 in the polymeric membrane matrix promoted the increase of EWC, ε and r_m for the nanocomposite membranes in comparison with pristine PEN membrane. When the zwitterionic nano-SiO_2 content varied from 0 to 0.5 wt%, the EWC, ε and r_m of prepared membranes increased from 73.7 to 83.0%, 66.5 to 76.1% and 42.4 to 52.1 nm, respectively. The increase in porosity of the nanocomposite membranes could be attributed to two aspects. Firstly, the incorporation of zwitterionic nano-SiO_2 could increase the thermodynamic instability of the casting solution which accelerated the exchange rate of solvent and non-solvent and promoted the formation of macrovoids during the phase inversion process;[59,60] secondly, the presence of zwitterionic nano-SiO_2 in polymer continuous phase of the nanocomposite membranes increased the structural heterogeneity of those membranes which leaded to the formation of more macrovoids to accommodate more water.[61,62] However, with the further increase of zwitterionic nano-SiO_2 content to 1 wt%, the agglomeration of nanoparticles weakened its effect on the thermodynamic instability of the casting solution, and the slower exchange rate of solvent and non-solvent eventually leaded to the PEN-1.0 with reduced EWC, ε and r_m, respectively.

3.4. Membrane separation performance

Fig. 8 presents the PWF, permeation flux and BSA rejection ratio of prepared membrane. A trade-off between flux and selectivity of composite membranes have been found. With the addition of zwitterionic nano-SiO_2 from 0 to 0.5 wt%, the PWF and permeation flux of the prepared composite membrane gradually increased, while the corresponding BSA rejection ratio gradually decreased. This exactly coincided with the tendency of porosity and r_m of the composite membrane surface from small to large. These results demonstrated that the increase in porosity and r_m of composite membrane with 0–0.5 wt% zwitterionic nano-SiO_2 content could attract water molecules inside the membrane matrix and promoted the passage of water molecules through the membrane to increase the permeability.[63] However, further increasing zwitterionic nano-SiO_2 content to 1 wt%, both the flux and selectivity of prepared composite membrane decreased. This could be explained by the fact that the particle agglomeration caused by excessive addition of nanoparticles might cause the blockage of the membrane pores, and ultimately leaded to the reducing of separation performance.[64] An optimal performance of PWF (507.2 L m^{-2} h^{-1}), permeation flux (247.1 L m^{-2} h^{-1}) and BSA rejection ratio (97.4%) was obtained when the addition of zwitterionic nano-SiO_2 reached 0.5 wt%.

The effect of the added zwitterionic nano-SiO_2 content on P_m of the prepared nanocomposite membrane was shown in Fig. 9 and the specific P_m value was calculated by eqn (7). With the incorporation of zwitterionic nano-SiO_2 increased from 0 to 0.5 wt%, the P_m of the nanocomposite membrane increased from 1.97 to 3.89, which mean the permeability enhanced with increasing the concentration of zwitterionic nano-SiO_2. This improvement in permeability could be attributed to the higher

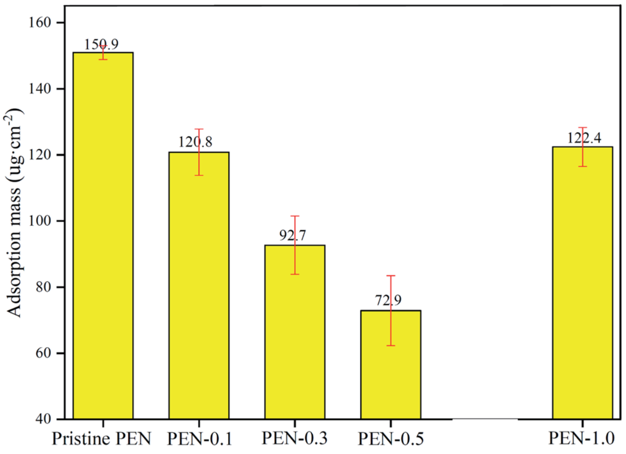

Fig. 11 Static adsorption of BSA solution of pristine PEN and nanocomposite membranes.

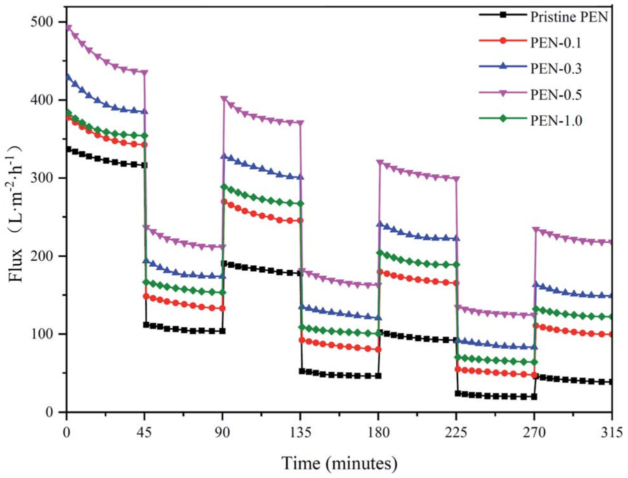

Fig. 12 Time-dependent fluctuation of pure water flux and BSA solution flux in three cycles.

porosity with addition of zwitterionic nano-SiO_2 in the polymer matrix. When modified SiO_2 nanoparticles content further increased to 1.0 wt%, P_m decreased to 3.14 instead, which mean that an excessive filler content would lead to a particle agglomeration, blocking the membrane pores that prevented the passage of water flow.[65,66]

3.5. Membrane hydrophilicity and anti-fouling performance

The water contact angle (WCA) and surface energy (γ) tests were used to evaluate the hydrophilicity and wettability of membranes. Generally, membranes with lower WCA or higher γ have more hydrophilic membrane surfaces.[67,68] Fig. 10 showed that pristine PEN had highest WCA of 81.3° and lowest γ of 41.3 mJ m^{-2}, while with the gradual addition of zwitterionic nano-SiO_2 to 0.5 wt%, the WCA decreased to 58.4° and γ increased to 55.4 mJ m^{-2}. This result indicated that the addition of zwitterionic nano-SiO_2 effectively improved the hydrophilicity of nanocomposite membrane surface. Hydroxyl functional group rich in the SiO_2 nanoparticle surface could bind more water molecules through hydrogen bonding, thereby increasing the wettability of the nanocomposite membrane.[63] When the content of zwitterionic nano-SiO_2 reached 1.0 wt%, the uneven distribution of nanoparticles on membrane surface caused the hydrophilicity of PEN-1.0 decreased.

The static fouling adsorption experiment results of pristine and nanocomposite PEN membranes were shown in Fig. 11. All PEN MMMs modified with zwitterionic SiO_2 NPs nanocomposites exhibited lower BSA adsorption capacity than pristine PEN membrane (150.9 μg cm^{-2}). The presence of zwitterionic SiO_2 NPs on the surface of PEN nanocomposite membranes were beneficial to the formation of a tight hydration layer on the membrane surface, thereby further weakened the specific adsorption of BSA on the membrane surface.[69] BSA adsorption amount of PEN-0.5 was only 72.9 μg cm^{-2}, which was the lowest among all PEN MMMs.

It is well known that membrane fouling will reduce the membrane permeability and shorten the usage time.[70] The time dependent flux of pristine PEN and nanocomposite membranes were conducted to evaluate the effect of adding zwitterionic nano-SiO_2 on antifouling performance, and the results were shown in Fig. 12. A significant flux drop occurred when the pure water feed was replaced by BSA solution due to larger size contaminants sticking to and blocking the pore of membrane surface.[71] After the membrane was thoroughly washed and backwashed, the PWF was measured again in order to determine the restoration ability and contribution of R_r and R_{ir} in R_t of each membrane. The PWF of all membranes could not be fully recovered due to the irreversible fouling.[72]

As shown in Fig. 13a, the antifouling effect of nanocomposite membrane was significantly improved compared to pristine PEN. With the increase in modified nanoparticles content, the nanocomposite membranes had higher FRR, R_r and lower R_t, R_{ir}, especially PEN-0.5 has an FRR of up to 85.3%. This could be explained as the content of hydroxyl groups on the membrane surface increased with the addition of zwitterions nano-SiO_2, making it easier to bind water molecules through hydrogen bonding by forming a hydrated layer on the membrane surface and effectively inhibit the adhesion of BSA on the membrane surface to reduce the total pollution degree.[73,74] Simultaneously, under the same cleaning conditions, the contamination of

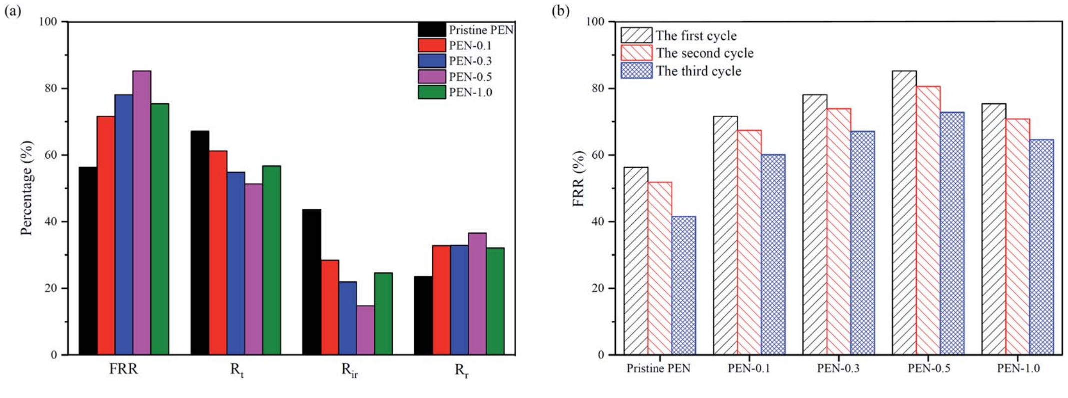

Fig. 13 (a) Anti-fouling parameters in the first cycle and (b) the FRR of the membranes in three cycles.

Table 3 Pure water flux, BSA rejection ratio and FRR comparison of nanocomposite UF membranes

Hybrid membrane	Operating pressure (bar)	PWF (L m^{-2} h^{-1})	Rejection (%)	FRR (%)	Ref.
PVDF/TiO_2	1	103.5	85.6	96.9	Moghadam *et al.*[78]
PES/PHEMA@SiO_2	2	141.7	95.0	84.4	Zhu *et al.*[79]
PSF/ONC	1	307	97.6	89	Khan *et al.*[80]
PVDF-OMW-GO	1	203	81.4	80.4	Zhang *et al.*[81]
PSf/SiO_2-GO	1	375	98	72	Wu *et al.*[82]
PES/HANTs-DA-TA	1	439	97	77.9	Mu *et al.*[55]
PSf/TiO_2-PDA	2	428	89	80	Wu *et al.*[83]
PEN-0.5	1	507.2	97.4	85.3	This work

Table 4 Mechanical strength of pristine PEN and nanocomposite membranes

Membranes	Breaking strength (mPa)	Elongation at break (%)
Pristine PEN	5.42 ± 0.27	23.60 ± 1.50
PEN-0.1	6.03 ± 0.15	27.22 ± 2.09
PEN-0.3	6.67 ± 0.22	28.74 ± 1.95
PEN-0.5	5.60 ± 0.12	28.96 ± 1.06
PEN-1.0	4.53 ± 0.11	20.38 ± 0.42

membrane surface with hydrated layer was easier washed away and the FRR increased.[75] When the content of nanoparticles continued to increase to 1.0 wt%, the hydrophobic modification effect was reduced due to the agglomeration of nanoparticles on the membrane surface. The pure water flux recovery under three cycles was shown in Fig. 13b. The FRR of all membranes showed a downward trend with increasing the cycles, namely $FRR_{1st} > FRR_{2st} > FRR_{3st}$. As the cycles increased, the interaction between the membrane surface protein and protein in the solution became stronger. The protein in the solution was more likely to directly interact with the membrane surface protein to deposit on the membrane surface. The total pollution degree of the membrane surface increased, the cleaning difficulty increased, and the flux recovery rate further decreased.[76,77]

As listed in Table 3, the overall performance of PEN hybrid membrane with optimum zwitterionic SiO_2 NPs content (0.5 wt%) was compared with other inorganic nanocomposite membranes published. The PEN-0.5 showed better performance in terms of pure water flux, rejection of BSA and flux recovery ratio. We think that zwitterionic SiO_2 NPs was a promising nanofiller used to prepared antifouling PEN ultrafiltration membranes.

3.6. Membrane mechanical properties

The mechanical strength of pressure driven UF membrane was crucial to ensure long-term stable operation under pressure. The mechanical performance parameters of pristine PEN and nanocomposite membranes were listed in Table 4. Compared with pristine PEN, when the addition of zwitterionic nanoparticles did not exceed 0.3 wt%, the breaking strength of the prepared nanocomposite membranes were significantly improved, and the change of breaking elongation was small. The improved mechanical strength of nanocomposite membranes could be attributed to the both synergistic effect of the good dispersion stability of nano-SiO_2 in the membrane matrix and the hydrogen bond between the hydroxyl group of silica surface and the PEN molecular chain as shown in Fig. 14. With further increasing nanoparticles content, the mechanical properties of nanocomposite membranes decreased significantly. This could be caused by the easier formation of stress concentration points in the membrane matrix under the action of external forces by the agglomeration of nanoparticles.

4. Conclusions

In this study, zwitterionic nano-SiO_2 was successfully prepared and used as filler to prepare PEN/zwitterionic nano-SiO_2 composite membranes by immersion precipitation phase inversion method. The effect of zwitterionic nano-SiO_2 addition amount on the structure and performance of PEN/zwitterionic nano-SiO_2 composite membrane was studied. With the optimum addition amount of zwitterionic nano-SiO_2 of 0.5 wt%, the prepared PEN/zwitterionic nano-SiO_2 composite membrane PEN-0.5 showed PWF of 507.2 L m^{-2} h^{-1}, permeation flux of 247.1 L m^{-2} h^{-1} and BSA rejection ratio of 97.4%.

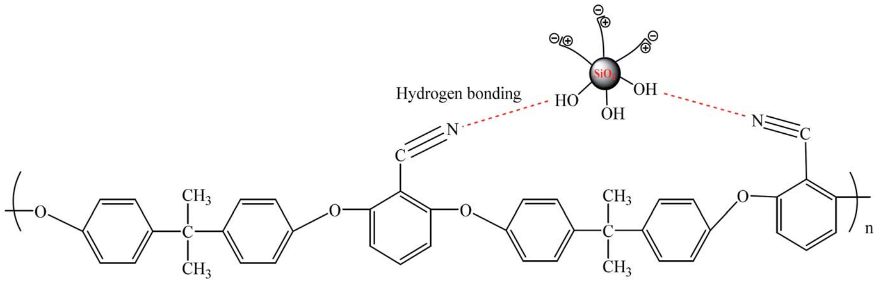

Fig. 14 The schematic diagram of the hydrogen bond interaction between zwitterionic SiO_2 NPs and PEN molecular chain.

Compared with pristine PEN, the porosity, EWC of PEN-0.5 had been significantly improved, the WCA decreased from 81.3° to 58.4°, meanwhile the surface energy increased from 41.3 to 55.4 mJ m^{-2}. In addition, PEN-0.5 exhibited a static adsorption capacity of 72.9 μg cm^{-2} which was less than half of pristine PEN, and the FRR under dynamic antifouling experiment was as high as 85.3%. The excellent antifouling performance of PEN/zwitterionic nano-SiO_2 nanocomposite membranes indicates that the blending modification with zwitterionic nano-SiO_2 is an effective and convenient method to enhance the permeability and antifouling performance of PEN membranes.

Conflicts of interest

The authors declare that they have no known competing financial interests or personal relationships that could have appeared to influence the work reported in this paper.

Acknowledgements

This work was supported by Research Startup program of Donghua University (285-07-005702) and the Key-Area Research and Development Program of Guangdong Province (2020B010182002).

References

1 A. Barbetta, M. Dentini, E. M. Zannoni and M. E. D. Stefano, Tailoring the porosity and morphology of gelatin-methacrylate polyHIPE scaffolds for tissue engineering applications, *Langmuir*, 2005, **21**(26), 12333–12341.

2 Y. Pan, Z. X. Yu, H. Shi, Q. Chen, G. Y. Zeng, H. H. Di, X. Q. Ren and Y. He, A novel antifouling and antibacterial surface-functionalized PVDF ultrafiltration membrane *via* binding Ag/SiO_2 nanocomposites, *J. Chem. Technol. Biotechnol.*, 2017, **92**(3), 552–562.

3 W. Dan and M. R. Bird, The fouling and cleaning of ultrafiltration membranes during the filtration of model tea component solutions, *J. Food Process Eng.*, 2007, **30**(3), 293–323.

4 H. S. Thiam, W. R. W. Daud, S. K. Kamarudin, A. B. Mohammad, A. A. H. Kadhum, K. S. Loh and E. H. Majlan, Overview on nanostructured membrane in fuel cell applications, *Int. J. Hydrogen Energy*, 2011, **36**(4), 3187–3205.

5 D. Song, J. Xu, Y. P. Fu, L. Xu and B. T. Shan, Polysulfone/sulfonated polysulfone alloy membranes with an improved performance in processing mariculture wastewater, *Chem. Eng. J.*, 2016, **304**(11), 882–889.

6 B. E. Logan and M. Elimelech, Membrane-based processes for sustainable power generation using water, *Nature*, 2012, **488**(7411), 313–319.

7 M. Ulbricht, Advanced functional polymer membranes, *Polymer*, 2006, **47**(7), 2217–2262.

8 Z. Yi, L. P. Zhu, L. Cheng, B. K. Zhu and Y. Y. Xu, A readily modified polyethersulfone with amino-substituted groups: its amphiphilic copolymer synthesis and membrane application, *Polymer*, 2012, **52**(2), 350–358.

9 W. Gao, H. Liang, J. Ma, M. Han, Z. L. Chen, Z. S. Han and G. B. Li, Membrane fouling control in ultrafiltration technology for drinking water production: a review, *Desalination*, 2011, **272**(1–3), 1–8.

10 S. S. Kulkarni, E. W. Funk and N. N. Li, *Introduction and Definitions. In: Membrane Handbook*, Springer, 1992, DOI: 10.1007/978-1-4615-3548-5-26.

11 I. G. P. Syed, A. M. Isloor, Inamuddin, A. M. Asiri, A. F. Ismail, R. Kumar and M. I. Ahamed, Performance intensification of the polysulfone ultrafiltration membrane by blending with copolymer encompassing novel derivative of poly(styrene-*co*-maleic anhydride) for heavy metal removal from wastewater, *Chem. Eng. J.*, 2018, **353**(12), 425–435.

12 I. K. Moideen, A. M. Isloor, B. Garudachari and A. F. Ismail, The effect of glycine betaine additive on the PPSU/PSF ultrafiltration membrane performance, *Desalin. Water Treat.*, 2016, **57**(52), 24788–24798.

13 D. P. Liu, T. B. Wang and C. J. He, Antifouling polyethersulfone membrane blended with a dual-mode amphiphilic copolymer, *J. Mater. Sci.*, 2016, **51**(16), 7383–7394.

14 M. O. Mavukkandy, M. R. Bilad, A. Giwa, S. W. Hasan and H. A. Arafat, Leaching of PVP from PVDF/PVP blend membranes: impacts on membrane structure and fouling in membrane bioreactors, *J. Mater. Sci.*, 2016, **51**(9), 1–14.

15 G. G. Shi, Y. Q. Shen, P. Mu, Q. T. Wang, Y. X. Yang, S. Y. Ma and J. Li, Effective separation of surfactant-stabilized crude oil-in-water emulsions by using waste brick powder-coated membranes under corrosive conditions, *Green Chem.*, 2020, **22**(4), 1345–1352.

16 H. J. Zhang, Y. Q. Shen, M. J. Li, G. R. Zhu, H. Feng and J. Li, Egg shell powders-coated membrane for surfactant-stabilized crude oil-in-water emulsions efficient separation, *ACS Sustainable Chem. Eng.*, 2019, **7**(12), 10880–10887.

17 C. Li, S. X. Li, L. Lv, B. W. Su and M. Z. Hu, High solvent-resistant and integrally crosslinked polyimide-based composite membranes for organic solvent nanofiltration, *J. Membr. Sci.*, 2018, **564**, 10–21.

18 M. Hossein and B. Rafie, Cellulose acetate/SiO_2-poly(2-acrylamido-2-methylpropane sulfonic acid) hybrid nanofiltration membrane: application in removal of ceftriaxone sodium, *J. Iran. Chem. Soc.*, 2018, **15**(12), 2839–2849.

19 H. Y. Li, P. Mu, J. Li and Q. Wang, Inverse desert beetle-like ZIF-8/PAN composite nanofibrous membrane for highly efficient separation of oil-in-water emulsions, *J. Mater. Chem. A*, 2021, **9**(7), 4167–4175.

20 V. L. Rao, A. Saxena and K. N. Ninan, Poly(arylene ether nitrile) (PEN), *J. Macromol. Sci., Polym. Rev.*, 2002, **42**(4), 513–540.

21 Y. Q. Zhao, Y. J. Lei, F. B. Meng, J. C. Zhong, R. Zhao and X. B. Liu, Electrical, thermal, and mechanical properties of polyarylene ether nitriles/graphite nanosheets

nanocomposites prepared by masterbatch route, *J. Mater. Sci.*, 2011, **46**(3), 824–831.

22 Y. You, S. N. Liu, L. Tu, Y. J. Wang, C. H. Zhan, X. Y. Du, R. B. Wei and X. B. Liu, Controllable fabrication of poly(arylene ether nitrile) dielectrics for thermal-resistant film capacitors, *Macromolecules*, 2019, **52**(15), 5850–5859.

23 Y. Q. Zhan, S. J. He, X. Y. Wan, S. M. Zhao and Y. L. Bai, Thermally and chemically stable poly(arylene ether nitrile)/halloysite nanotubes intercalated graphene oxide nanofibrous composite membranes for highly efficient oil/water emulsion separation in harsh environment, *J. Membr. Sci.*, 2018, **567**, 76–88.

24 W. L. Zhang, Z. J. Wang and X. B. Liu, A novel poly(arylene ether nitrile) ultrafiltration membrane for water purification and its antifouling property with *in situ*-generated SiO_2 nanoparticles, *High Perform. Polym.*, 2019, **31**(8), 977–985.

25 W. Gao, H. Liang, J. Ma, H. Mei, Z. L. Chen, Z. S. Han and G. B. Li, Membrane fouling control in ultrafiltration technology for drinking water production: a review, *Desalination*, 2011, **272**(1–3), 1–8.

26 I. Banerjee, R. C. Pangule and R. S. Kane, Antifouling Coatings: Recent Developments in the Design of Surfaces That Prevent Fouling by Proteins, Bacteria, and Marine Organisms, *Adv. Mater.*, 2011, **23**(6), 690–718.

27 L. Braeken, B. Bettens, K. Boussu, P. V. D. Meeren, J. Cocquyt, J. Vermant and B. V. D. Bruggen, Transport mechanisms of dissolved organic compounds in aqueous solution during nanofiltration, *J. Membr. Sci.*, 2006, **279**(1–2), 311–319.

28 A. K. Wardani, D. Ariono, Subagjo and I. G. Wenten, Hydrophilic modification of polypropylene ultrafiltration membrane by air-assisted polydopamine coating, *Polym. Adv. Technol.*, 2019, **30**(4), 1148–1155.

29 H. G. Sun, X. B. Yang, Y. Q. Zhang, X. Q. Cheng, Y. C. Xu, Y. P. Bai and L. Shao, Segregation-induced *in situ* hydrophilic modification of poly(vinylidene fluoride) ultrafiltration membranes *via* sticky poly(ethylene glycol) blending, *J. Membr. Sci.*, 2018, **563**, 22–30.

30 A. F. Ismail, C. S. Ong, N. Misdan and W. J. Lau, Nanomaterials for biofouling and scaling mitigation of thin film composite membrane: a review, *Desalination*, 2016, **393**(SI), 2–5.

31 H. X. Yu, L. Gu, S. F. Wu, G. X. Dong, X. B. Qiao, K. Zhang, X. Y. Lu, H. F. Wen and D. F. Zhang, Hydrothermal carbon nanospheres assisted-fabrication of PVDF ultrafiltration membranes with improved hydrophilicity and antifouling performance, *Sep. Purif. Technol.*, 2020, **247**, 116889.

32 A. V. R. Reddy, D. J. Mohan, A. Bhattacharya, V. J. Shah and P. K. Ghosh, Surface modification of ultrafiltration membranes by preadsorption of a negatively charged polymer I. Permeation of water soluble polymers and inorganic salt solutions and fouling resistance properties, *J. Membr. Sci.*, 2003, **214**(2), 211–221.

33 H. Y. Yu, Z. K. Xu, Y. J. Xie, Z. M. Liu and S. Y. Wang, Flux enhancement for polypropylene microporous membrane in a SMBR by the immobilization of poly(*N*-vinyl-2-pyrrolidone) on the membrane surface, *J. Membr. Sci.*, 2006, **279**(1–2), 148–155.

34 Y. Liu, S. L. Zhang and G. B. Wang, The preparation of antifouling ultrafiltration membrane by surface grafting zwitterionic polymer onto poly(arylene ether sulfone) containing hydroxyl groups membrane, *Desalination*, 2013, **316**, 127–136.

35 R. K. Du, B. J. Gao and Y. B. Li, Hydrophilic polysulfone film prepared from polyethylene glycol monomethylether *via* coupling graft, *Appl. Surf. Sci.*, 2013, **274**(1), 288–294.

36 S. L. Yu, X. T. Zuo, R. L. Bao, X. Xu, J. Wang and J. Xu, Effect of SiO_2 nanoparticle addition on the characteristics of a new organic–inorganic hybrid membrane, *Polymer*, 2009, **50**(2), 553–559.

37 M. Obaid, G. M. K. Tolba, M. Motlak, O. A. Fadali, K. A. Khalil, A. A. Almajid, B. Kim and N. A. M. Barakat, Effective polysulfone-amorphous SiO_2 NPs electrospun nanofiber membrane for high flux oil/water separation, *Chem. Eng. J.*, 2015, **279**, 631–638.

38 M. Parimalam, M. R. Islam and R. M. Yunus, Effects of nanosilica and titanium oxide on the performance of epoxy–amine nanocoatings, *J. Appl. Polym. Sci.*, 2019, **136**(35), 47901.

39 J. H. So, S. M. Yang, C. Y. Kim and J. C. Hyun, Microstructure and rheological behaviour of electrosterically stabilized silica particle suspensions, *Colloids Surf., A*, 2001, **190**(1–2), 89–98.

40 A. B. Lowe and C. L. Mccormick, Synthesis and solution properties of zwitterionic polymers, *Chem. Rev.*, 2002, **102**(11), 4177–4189.

41 A. Islam, J. G. Li, M. Pervaiz, Z. H. Lu, M. Sain, L. H. Chen and X. H. Ouyang, Zwitterions for Organic/Perovskite Solar Cells, Light-Emitting Devices, and Lithium Ion Batteries: Recent Progress and Perspectives, *Adv. Energy Mater.*, 2019, **9**, 1803354.

42 J. Zhao, M. Milanova, M. M. C. G. Warmoeskerken and V. Dutschk, Surface modification of TiO_2 nanoparticles with silane coupling agents, *Colloids Surf., A*, 2012, **413**, 273–279.

43 X. G. Li, Y. Q. He and M. T. Swihart, Surface functionalization of silicon nanoparticles produced by laser-driven pyrolysis of silane followed by HF-HNO_3 etching, *Langmuir*, 2004, **20**(11), 4720–4727.

44 J. Zhao, M. Milanova, M. M. C. G. Warmoeskerken and V. Dutschk, Surface modification of TiO_2 nanoparticles with silane coupling agents, *Colloids Surf., A*, 2012, **413**, 273–279.

45 X. G. Li, Y. Q. He and M. T. Swihart, Surface functionalization of silicon nanoparticles produced by laser-driven pyrolysis of silane followed by HF-HNO_3 etching, *Langmuir*, 2004, **20**(11), 4720–4727.

46 R. C. Su, W. F. Li, J. Peng and D. Jun, Surface modification of nano-sized SiO_2 with silane coupling agent and its dispersion, *Chem. Ind. Eng. Prog.*, 2009, **28**(9), 1596–1603.

47 L. Y. Jiang, C. M. Leu and H. K. Wei, Layered silicates/fluorinated polyimide nanocomposites for advanced

dielectric materials applications, *Adv. Mater.*, 2002, **14**(6), 426–429.

48 Y. X. Zhang, Y. L. Liu, B. Q. Ren, D. Zhang and J. Zheng, Fundamentals and applications of zwitterionic antifouling polymers, *J. Phys. D: Appl. Phys.*, 2019, **52**, 403001.

49 J. Zhu, X. Z. Zhao and C. J. He, Zwitterionic SiO_2 nanoparticles as novel additives to improve the antifouling properties of PVDF membranes, *RSC Adv.*, 2015, **5**(66), 53653–53659.

50 H. Tang, J. Yang, J. Zhong, R. Zhao and X. Liu, Synthesis and dielectric properties of polyarylene ether nitriles with high thermal stability and high mechanical strength, *Mater. Lett.*, 2011, **65**(17–18), 2758–2761.

51 J. T. Mao, H. P. Yang, Z. Gao, R. C. Zhang and S. Q. Chai, Study on photacatalysis and separation performance of KH550-TiO_2 immobilized on PES ultrafiltration membrane, *Environ. Sci. Technol.*, 2018, **31**(4), 7–13.

52 Y. N. Yang, W. Jun, Q. Z. Zheng, X. S. Chen and H. X. Zhang, The research of rheology and thermodynamics of organic–inorganic hybrid membrane during the membrane formation, *J. Membr. Sci.*, 2008, **311**(1–2), 200–207.

53 Y. N. Yang, H. X. Zhang, P. Wang, Q. Z. Zheng and J. Li, The influence of nano-sized TiO_2 fillers on the morphologies and properties of PSF UF membrane, *J. Membr. Sci.*, 2007, **288**(1–2), 231–238.

54 W. Z. Lang, Q. Ji, J. P. Shen, Y. J. Guo and L. F. Chu, Modified poly(vinylidene fluoride) hollow fiber composite membranes reinforced by hydroxyapatite nanocrystal whiskers, *J. Appl. Polym. Sci.*, 2013, **127**(6), 4564–4572.

55 Y. F. Mu, K. Zhu, J. S. Luan, S. L. Zhang, C. Y. Zhang, R. Q. Na, Y. C. Yang, X. Zhang and G. B. Wang, Fabrication of hybrid ultrafiltration membranes with improved water separation properties by incorporating environmentally friendly taurine modified hydroxyapatite nanotubes, *J. Membr. Sci.*, 2019, **577**, 274–284.

56 M. L. Luo, J. Q. Zhao, W. Tang and C. S. Pu, Hydrophilic modification of poly(ether sulfone) ultrafiltration membrane surface by self-assembly of TiO_2 nanoparticles, *Appl. Surf. Sci.*, 2005, **249**(1–4), 76–84.

57 Manorma, I. Ferreira, P. Alves, M. H. Gil and L. M. G. Ferreira, Lignin separation from black liquor by mixed matrix polysulfone nanofiltration membrane filled with multiwalled carbon nanotubes, *Sep. Purif. Technol.*, 2021, **260**, 118231.

58 B. Chakrabarty, A. K. Ghoshal and M. K. Purkait, Effect of molecular weight of PEG on membrane morphology and transport properties, *J. Membr. Sci.*, 2008, **309**(1–2), 209–221.

59 J. Q. Zhao, H. R. Han, Q. Q. Wang, C. Y. Yan, Y. Li, J. Yang, X. Feng, N. Yang, Y. P. Zhao and L. Chen, Hydrophilic and anti-fouling PVDF blend ultrafiltration membranes using polyacryloylmorpholine-based triblock copolymers as amphiphilic modifiers, *React. Funct. Polym.*, 2019, **139**(1), 92–101.

60 J. Q. Zhao, Q. Q. Wang, J. Yang, Y. Li, Z. Y. Liu, L. Q. Zhang, Y. P. Zhao, S. X. Zhang and L. Chen, Comb-shaped amphiphilic triblock copolymers blend PVDF membranes overcome the permeability-selectivity trade-off for protein separation, *Sep. Purif. Technol.*, 2020, **239**, 116596.

61 P. Daraei, S. S. Madaeni, N. Ghaemi, E. Salehi, M. A. Khadivi, R. Moradian and B. Astinchap, Novel polyethersulfone nanocomposite membrane prepared by PANI/Fe_3O_4 nanoparticles with enhanced performance for Cu(ii) removal from water, *J. Membr. Sci.*, 2012, **415**, 250–259.

62 E. Bagheripour, A. R. Moghadassi, S. M. Hosseini, M. B. Ray, F. Parvizian and B. V. D. Bruggen, Highly hydrophilic and antifouling nanofiltration membrane incorporated with water-dispersible composite activated carbon/chitosan nanoparticles, *Chem. Eng. Res. Des.*, 2018, **132**, 812–821.

63 A. L. Ohland, V. M. M. Salim and C. P. Borges, Nanocomposite membranes for osmotic processes: incorporation of functionalized hydroxyapatite in porous substrate and in selective layer, *Desalination*, 2019, **463**, 23–31.

64 H. Rabiee, V. Vatanpour, M. H. D. A. Farahani and H. Zarrabi, Improvement in flux and antifouling properties of PVC ultrafiltration membranes by incorporation of zinc oxide (ZnO) nanoparticles, *Sep. Purif. Technol.*, 2015, **156**, 299–310.

65 L. Wang, X. J. Song, T. Wang, S. Z. Wang, Z. Wang and C. J. Gao, Fabrication and characterization of polyethersulfone/carbon nanotubes (PES/CNTs) based mixed matrix membranes (MMMs) for nanofiltration application, *Appl. Surf. Sci.*, 2015, **330**, 118–125.

66 J. H. Choi, J. Jegal and W. N. Kim, Fabrication and characterization of multi-walled carbon nanotubes/polymer blend membranes, *J. Membr. Sci.*, 2006, **284**(1–2), 406–415.

67 Y. Q. Zhang and P. L. Liu, Polysulfone(PSF) composite membrane with micro-reaction locations (MRLs) made by doping sulfated TiO_2 deposited on SiO_2 nanotubes (STSNs) for cleaning wastewater, *J. Membr. Sci.*, 2015, **493**, 275–284.

68 S. J. Yang, Q. F. Zou, T. H. Wang and L. P. Zhang, Effects of GO and MOF@GO on the permeation and antifouling properties of cellulose acetate ultrafiltration membrane, *J. Membr. Sci.*, 2019, **569**, 48–59.

69 L. M. Bai, H. Y. Wu, J. W. Ding, A. Ding, X. Y. Zhang, N. Q. Ren, G. B. Li and H. Liang, Cellulose nanocrystal-blended polyethersulfone membranes for enhanced removal of natural organic matter and alleviation of membrane fouling, *Chem. Eng. J.*, 2020, **382**, 122919.

70 A. Asatekin, S. Kang, M. Elimelech and A. M. Mayes, Anti-fouling ultrafiltration membranes containing polyacrylonitrile-*graft*-poly(ethylene oxide) comb copolymer additives, *J. Membr. Sci.*, 2007, **298**(1–2), 136–146.

71 Z. X. Liu, Z. M. Mi, C. H. Chen, H. W. Zhou, X. G. Zhao and D. M. Wang, Preparation of hydrophilic and antifouling polysulfone ultrafiltration membrane derived from phenolphthalin by copolymerization method, *Appl. Surf. Sci.*, 2017, **401**, 69–78.

72 M. Pirsaheb, M. H. D. A. Farahani, S. Zinadini, A. A. Zinatizadeh, M. Rahimi and V. Vatanpour, Fabrication of high-performance antibiofouling ultrafiltration membranes with potential application in membrane bioreactors (MBRs) comprising

polyethersulfone (PES) and polycitrate-Alumoxane (PC-A), *Sep. Purif. Technol.*, 2019, **211**, 618–627.

73 H. G. Sun, X. B. Yang, Y. Q. Zhang, X. Q. Cheng, Y. C. Xu, Y. P. Bai and L. Shao, Segregation-induced *in situ* hydrophilic modification of poly(vinylidene fluoride) ultrafiltration membranes *via* sticky poly(ethylene glycol) blending, *J. Membr. Sci.*, 2018, **563**, 22–30.

74 J. R. Werber, C. O. Osuji and M. Elimelech, Materials for next-generation desalination and water purification membranes, *Nat. Rev. Mater.*, 2016, **1**(5), 18–22.

75 Y. F. Mu, H. Feng, S. L. Zhang, C. Y. Zhang, N. Lu, J. S. Luan and G. B. Wang, Development of highly permeable and antifouling ultrafiltration membranes based on the synergistic effect of carboxylated polysulfone and bio-inspired co-deposition modified hydroxyapatite nanotubes, *J. Colloid Interface Sci.*, 2020, **572**, 48–61.

76 M. S. S. A. Saraswathi, D. Rana, K. Divya, S. Alwarappan and A. Nagendran, Fabrication of anti-fouling PVDF nanocomposite membranes using manganese dioxide nanospheres with tailored morphology, hydrophilicity and permeation, *New J. Chem.*, 2018, **42**(19), 15803–15810.

77 M. Padaki, D. Emadzadeh, T. Masturra and A. F. Ismail, Antifouling properties of novel PSf and TNT composite membrane and study of effect of the flow direction on membrane washing, *Desalination*, 2015, **362**, 141–150.

78 M. T. Moghadam, G. Lesage, T. Mohammadi, J. P. Mericq, J. Mendret, M. Heran, C. Faur, S. Brosillon, M. Hemmati and F. Naeimpoor, Improved antifouling properties of TiO_2/PVDF nanocomposite membranes in UV-coupled ultrafiltration, *J. Appl. Polym. Sci.*, 2015, **132**(21), 41731.

79 L. J. Zhu, L. P. Zhu, J. H. Jiang, Z. Yi, Y. F. Zhao, B. K. Zhu and Y. Y. Xu, Hydrophilic and anti-fouling polyethersulfone ultrafiltration membranes with poly(2-hydroxyethyl methacrylate) grafted silica nanoparticles as additive, *J. Membr. Sci.*, 2014, **451**, 157–168.

80 A. Khan, T. A. Sherazi, Y. Khan, S. H. Li, S. A. R. Naqvi and Z. Cui, Fabrication and characterization of polysulfone/modified nanocarbon black composite antifouling ultrafiltration membranes, *J. Membr. Sci.*, 2018, **554**, 71–82.

81 J. G. Zhang, Z. W. Xu, W. Mai, C. Y. Min, B. M. Zhou, M. J. Shan, Y. L. Li, C. Y. Yang, Z. Wang and X. M. Qian, Improved hydrophilicity, permeability, antifouling and mechanical performance of PVDF composite ultrafiltration membranes tailored by oxidized low-dimensional carbon nanomaterials, *J. Mater. Chem. A*, 2013, **1**(9), 3101–3111.

82 H. Q. Wu, B. B. Tang and P. Y. Wu, Development of novel SiO_2-GO nanohybrid/polysulfone membrane with enhanced performance, *J. Membr. Sci.*, 2014, **451**, 94–102.

83 H. Q. Wu, Y. J. Liu, L. Mao, C. H. Jiang, J. M. Ang and X. H. Lu, Doping polysulfone ultrafiltration membrane with TiO_2-PDA nanohybrid for simultaneous self-cleaning and self-protection, *J. Membr. Sci.*, 2017, **532**, 20–29.